*HeilArchive* : Pages:1–20

**Original Research**

# Retardation Theory for Soluble Gas-Kick Transients: Similarity Laws and Effective Compressibility in Annular Multiphase Flow with Methane Dissolution

Vo Tuan[1] and Dang Quoc[2]

[1]Trường Đại học Quy Nhơn, Khoa Công nghệ Thông tin, 170 đường An Dương Vương, thành phố Quy Nhơn, Bình Định 820000, Việt Nam.
[2]Trường Đại học Hồng Đức, Khoa Công nghệ Thông tin và Truyền thông, 565 đường Quang Trung, phường Đông Vệ, thành phố Thanh Hóa 440000, Việt Nam.

**Abstract**
Gas influx into a drilling annulus remains a central safety concern because small downhole disturbances can transition into rapid surface transients as pressure decreases and methane expands. In synthetic and oil-based drilling fluids, a substantial fraction of methane mass may dissolve at depth, altering both the migration time scale and the mapping from total methane mass to surface indicators such as pit gain and wellhead pressure. Many operational analyses treat dissolution either as a binary switch or as an empirical delay, which obscures the mechanisms by which partitioning modifies compressibility, hydrostatic response, and observability. This paper develops a retardation-based theory for soluble gas-kick transients by deriving a reduced thermo-solutal model in which dissolved inventory acts as a dynamic buffer that slows the propagation of methane mass relative to free-gas holdup. The contribution is a unified set of similarity laws and effective-parameter representations that connect equilibrium solubility, finite-rate mass transfer, annular slip, and circulation into closed-form estimates of arrival time, indicator amplitude, and early-time detectability. The analysis yields an explicit retardation factor that modifies drift-flux transport and an effective mixture compressibility that quantifies how dissolution weakens surface sensitivity to influx during the early stage. A surface-signature inversion is then derived that reconstructs admissible influx histories from pressure and pit-volume observations while accounting for solubility-driven buffering and thermal variation. The resulting theory is intended to support real-time interpretation by providing mechanistic scaling relations, identifiability conditions, and physically constrained inversion operators that remain valid across non-circulating and circulating regimes under high-pressure high-temperature conditions.

## 1. Introduction

Transient gas-kick behavior in drilling annuli has traditionally been interpreted through the evolution of a small set of surface observables, notably pit-volume changes and wellhead pressure perturbations, combined with mechanistic reasoning about buoyant migration and compressibility [1]. The underlying physical system, however, is a distributed multiphase transport problem with strong coupling among pressure, temperature, density, and slip. In deep wells, the pressure field varies strongly with depth, and methane density can change by orders of magnitude along the ascent path, making even small free-gas holdup fractions dynamically important. At the same time, drilling operations impose boundary and interior perturbations through circulation rate changes, choke actions, and thermal drift, producing transients that can mask or imitate early kick signatures. In synthetic and oil-based drilling fluids, methane dissolution adds a further layer of complexity by allowing methane mass to be stored in the liquid phase at depth, reducing the amount of free gas that contributes to hydrostatic and frictional effects during early

stages [2]. This storage can delay the appearance of free-gas indicators without reducing the underlying methane mass hazard, and later exsolution can amplify surface response when equilibrium capacity decreases near the surface.

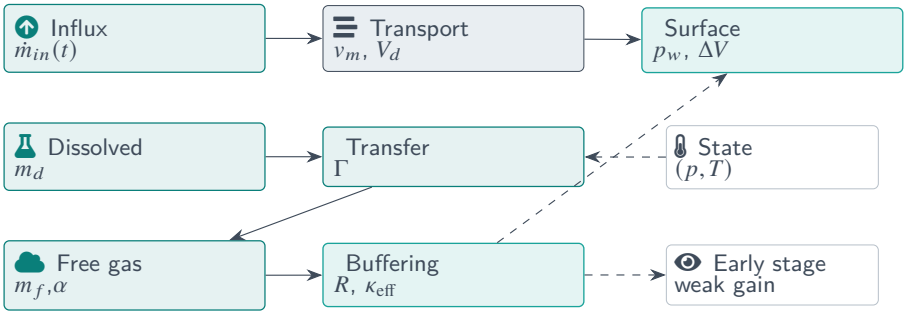


**Figure 1:** Compact signal chain: methane influx is transported upward while partitioning between dissolved and free inventories; thermo-solutal buffering compresses early surface response before exsolution strengthens $p_w$ and pit-gain signatures.

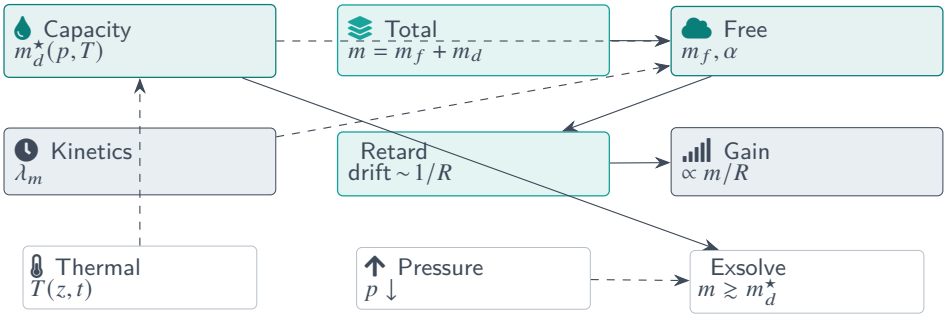


**Figure 2:** Thermo-solutal buffering in one glance: equilibrium capacity and finite-rate transfer regulate how much methane appears as free holdup, producing a retardation factor that weakens early indicator gain until exsolution becomes inevitable in upper low-pressure sections.

The technical difficulty of early interpretation can be stated as a problem of observability under strong nonlinear filtering. The downhole disturbance is the influx at depth, while the measurements are sparse

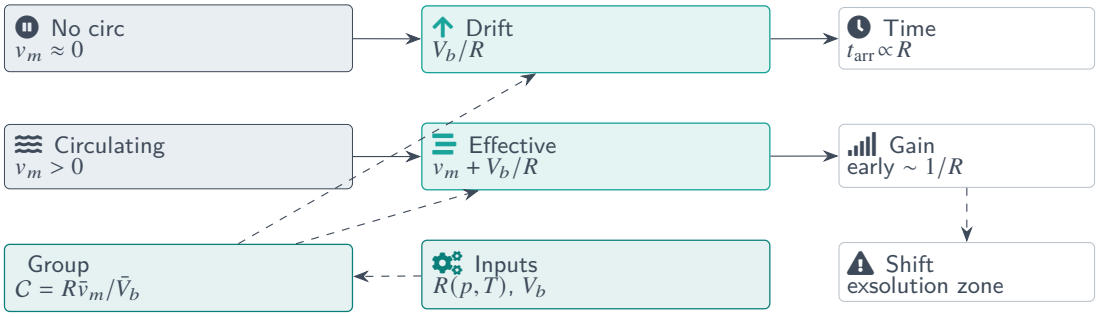


**Figure 3:** Similarity structure across operating regimes: retardation reduces drift speed and early signal gain; circulation can shorten travel time while the buffering factor still suppresses initial observability until exsolution strengthens the response.

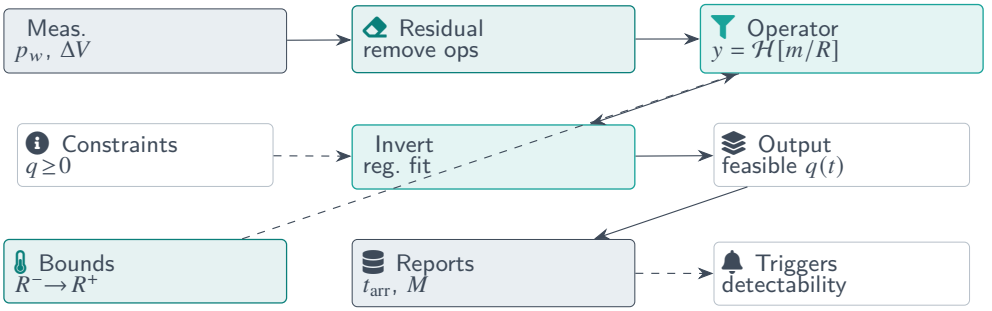


**Figure 4:** Surface-signature inversion with buffering: a compact residual indicator is mapped through a retarded observation operator and inverted under positivity/regularity constraints, while thermo-solutal uncertainty enters through bounded retardation intervals.

| Symbol | Meaning | Units |
|---|---|---|
| $z$ | Depth coordinate, $z \in [0, L]$ | m |
| $t$ | Time | s |
| $p(z,t)$ | Pressure | Pa |
| $T(z,t)$ | Temperature | K |
| $v_m(z,t)$ | Mixture superficial velocity | m/s |
| $\alpha(z,t)$ | Free-gas volume fraction | – |

**Table 1:** Primary field variables for the annular thermo-solutal model.

and typically available only at the surface. The mapping from influx to measurements is mediated by transport delays, by multiphase slip, by pressure-dependent density and dissolution capacity, and by uncertain closures for friction and bubble rise. Consequently, the same measured surface perturbation can correspond to multiple plausible downhole influx histories, particularly when dissolution buffers methane mass [3]. The goal of the present paper is not to improve a particular correlation or to advocate a particular simulator, but to derive a reduced theory that makes the buffering mechanism explicit and yields closed-form scaling relations that clarify when and how dissolution delays migration and weakens early detectability.

A common line of work in the literature treats early detection as a transient multiphase modeling problem, emphasizing how kick-induced perturbations propagate and how they might be distinguished

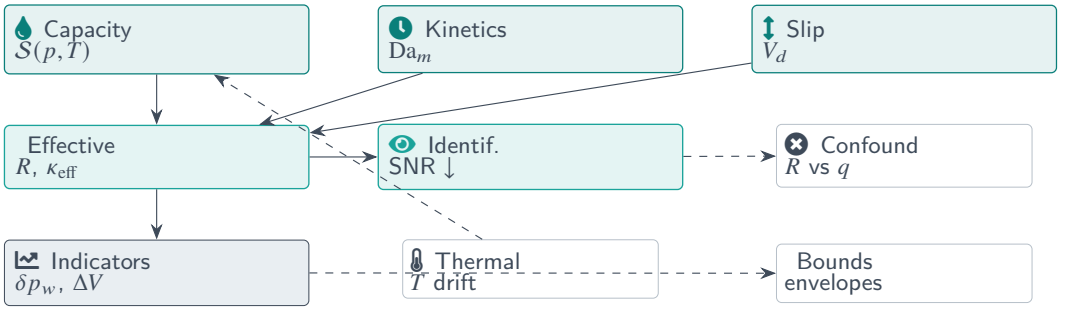


**Figure 5:** What controls early detectability: capacity, kinetics, and slip collapse into effective parameters that set both transport and signal gain; large buffering increases confounding between retardation and true influx magnitude, motivating conservative envelope reporting.

| Quantity | Definition | Interpretation |
|---|---|---|
| $m_f$ | $m_f = \alpha\rho_g$ | Free methane mass per mixture volume |
| $m_d$ | $m_d = (1-\alpha)\rho_\ell c$ | Dissolved methane mass per mixture volume |
| $m$ | $m = m_f + m_d$ | Total methane mass per mixture volume |
| $c$ | Dissolved methane concentration per unit liquid mass | State variable for liquid-phase methane |
| $c^\star$ | Equilibrium dissolved concentration $c^\star(p,T;\chi)$ | Solubility capacity at given $(p,T)$ |

**Table 2:** Methane inventory variables and their roles in the model.

from operational transients. A review focusing on early detection via transient multiphase flow modeling highlights that published models are predominantly one-dimensional and limited in the range of operating conditions, while also noting that solubility and heat transfer are often incorporated only partially and recommending more sophisticated modeling directions to improve prediction of phase velocities, temperature, and pressure patterns relevant to detection [4]. That perspective motivates fidelity improvements. The present paper develops a complementary perspective: even within a one-dimensional framework, a decisive mechanism for early-time behavior is the partitioning of methane between dissolved and free inventories, which can be treated analytically as a retardation phenomenon akin to sorption in porous-media transport [5]. This analogy is not invoked to suggest identical physics, but to emphasize that a dissolved inventory introduces a dynamic buffer that slows the propagation of methane mass relative to the free-gas signal that drives surface observables.

The central thesis is that soluble kick transients can be described, to leading order in relevant regimes, by a retarded drift-flux transport equation for a conserved methane mass variable, coupled to a fast equilibrium or finite-rate relaxation law that determines what fraction of that mass appears as free gas. In this description, the dissolved inventory does not merely delay a bubble front; it changes the effective compressibility of the mixture and thereby changes the sensitivity of surface observables to the underlying methane mass. The paper's technical contribution is a set of explicit scaling laws, similarity solutions, and inversion operators that quantify this effect across circulation regimes and that provide conditions under which early detection is intrinsically limited [6].

The work is organized around a sequence of reductions. A baseline drift-flux model with dissolved inventory is stated and non-dimensionalized to expose the controlling groups. A fast-equilibrium limit

| Balance | Schematic equation | Notes |
|---|---|---|
| Mixture mass | $\frac{\partial}{\partial t}(A\rho_m) + \frac{\partial}{\partial z}(A\rho_m v_m) = 0$ | Continuity of total fluid |
| Free methane | $\frac{\partial}{\partial t}(Am_f) + \frac{\partial}{\partial z}(Am_f v_g) = -A\Gamma + As_{in}$ | Free-gas transport and influx |
| Dissolved methane | $\frac{\partial}{\partial t}(Am_d) + \frac{\partial}{\partial z}(Am_d v_\ell) = A\Gamma$ | Liquid-phase storage and exchange |
| Momentum | $\frac{\partial}{\partial t}(A\rho_m v_m) + \frac{\partial}{\partial z}(A\rho_m v_m^2) + A\frac{\partial p}{\partial z} = -A\rho_m g\cos\theta - A\Delta_w$ | Compressible mixture momentum |
| Energy | $\frac{\partial}{\partial t}(A\rho_m h_m) + \frac{\partial}{\partial z}(A\rho_m v_m h_m) = -Av_m\frac{\partial p}{\partial z} + Aq_{\text{wall}}$ | Reduced thermal balance |

**Table 3:** Key governing equations used to derive the reduced retardation model.

| Symbol | Definition | Interpretation |
|---|---|---|
| $\tilde{z}$ | $\tilde{z} = z/L$ | Dimensionless depth |
| $\tilde{t}$ | $\tilde{t} = Ut/L$ | Dimensionless time |
| $\tilde{p}$ | $\tilde{p} = p/P$ | Dimensionless pressure |
| $\mathrm{Da}_m$ | $\mathrm{Da}_m = \lambda_{m,0}L/U$ | Mass-transfer Damköhler number |
| $\mathcal{S}$ | $\mathcal{S} = \rho_{\ell,0}c^\star/\rho_g$ | Solubility capacity ratio |
| $C$ | $C = R\,\bar{v}_m/\bar{V}_b$ | Circulation number (advection vs drift) |

**Table 4:** Representative dimensionless groups highlighting solubility and transport regimes.

| Regime | Defining condition | Dominant transport feature |
|---|---|---|
| Drift-dominated | $C \ll 1$ | Buoyant slip controls migration |
| Advection-dominated | $C \gg 1$ | Mixture advection controls migration |
| Fast equilibrium | $\mathrm{Da}_m \gg 1$ | $m_d \approx m_d^\star$ (strong buffering) |
| Finite-rate transfer | $\mathrm{Da}_m = O(1)$ | Time-varying retardation $R(z,t)$ |
| Slow transfer | $\mathrm{Da}_m \ll 1$ | Weak buffering, near-insoluble limit |

**Table 5:** Operational and thermo-solutal regimes relevant to methane-kick interpretation.

and an intermediate finite-rate regime are then analyzed to derive an effective retardation factor and an effective compressibility. These quantities are used to obtain closed-form ascent-time estimates and to derive linearized expressions for wellhead pressure and pit gain signatures in terms of retarded methane mass flux. Finally, a constrained inversion is developed that reconstructs admissible influx histories from surface observations while accounting for thermal variation and uncertain parameters through bounded operators [7]. The resulting theory is intended for use as an interpretive layer that can be embedded into

| Quantity | Expression | Effect on dynamics | Comment |
|---|---|---|---|
| $K$ | $K \approx m_d/m_f$ | Partition between dissolved and free methane | Large $K$ implies strong buffering |
| $R$ | $R = 1 + K$ | Retardation factor on drift | $R \geq 1$ slows mass relative to bubbles |
| $m_f$ | $m_f \approx m/R$ | Free methane for given total $m$ | Reduced free-gas inventory |
| $\alpha$ | $\alpha \approx m/(R\rho_g)$ | Free-gas volume fraction | Smaller holdup for large $R$ |
| $u_{\text{eff}}$ | $u_{\text{eff}} = v_m + V_b/R$ | Effective methane propagation velocity | Drift scaled by $1/R$ |
| $V_g$ | $V_g = \int_0^L A\alpha\, dz$ | Total free-gas volume | Drives volumetric surface response |

**Table 6:** Retardation-related quantities linking dissolution to transport and holdup.

| Case | Effective velocity | Arrival-time scaling | Comment |
|---|---|---|---|
| Shut-in (no circulation) | $u_{\text{eff}} \approx V_b/R$ | $t_{\text{arr}} \approx RL/V_b$ | Arrival slowed by retardation |
| Circulating, drift-relevant | $u_{\text{eff}} \approx \bar{v}_m + \bar{V}_b/R$ | $t_{\text{arr}} \approx L/u_{\text{eff}}$ | Both advection and drift matter |
| Strong circulation | $u_{\text{eff}} \approx \bar{v}_m$ | $t_{\text{arr}} \approx L/\bar{v}_m$ | $R$ mainly affects amplitude |
| Depth-varying profile | $u_{\text{eff}}(z)$ | $t_{\text{arr}} = \int_0^L dz/u_{\text{eff}}$ | Path-averaged effect of $R(z)$ |
| Onset of exsolution | – | $m(z_e, t) \approx m_d^\star(p, T)$ | Defines exsolution depth $z_e$ |

**Table 7:** Similarity laws for methane migration and arrival time across circulation regimes.

larger simulators or estimators, providing analytic insight and computationally cheap bounds rather than replacing full mechanistic models.

The narrative motivation for explicit dissolution treatment is grounded in the existence of mechanistic simulators that have demonstrated operationally relevant effects of methane solubility in non-aqueous drilling fluids. Manikonda et al. (2019) introduced an advanced semi-analytical model for annular gas kicks that incorporated methane solubility in oil-based drilling fluids and reported that soluble behavior can increase the time for gas to reach the wellhead relative to insoluble assumptions [8], underscoring that dissolution can reshape indicator timelines and should be treated as a primary mechanism rather than an auxiliary delay. The present paper does not attempt to reproduce such a simulator; it treats that observation as a constraint on any reduced theory, namely that a dissolution mechanism must appear explicitly and must act to retard the emergence of free gas and to weaken early surface sensitivity under high-pressure conditions.

## 2. Governing Model and Non-Dimensionalization

A one-dimensional annular model is formulated on a depth coordinate $z \in [0, L]$, where $z = 0$ corresponds to the wellhead and $z = L$ corresponds to the influx location or lower boundary of the modeled domain [9]. The annulus has cross-sectional area $A(z)$ and inclination $\theta(z)$, with $\theta = 0$ representing a

| Observable | Leading dependence | Sensitivity to $R$ | Inversion role |
|---|---|---|---|
| Wellhead pressure $\delta p_w$ | $-\int_0^L w_p\, m/(R\rho_g)\, dz$ | Magnitude $\propto 1/R$ | Hydrostatic indicator |
| Pit gain rate $\dot{V}_{\text{pit}}$ | $\dot{V}_{\text{pit}} \approx dV_g/dt$ | Early signal $\propto 1/R$ | Volumetric indicator |
| Free-gas volume $V_g$ | $V_g \approx \int_0^L Am/(R\rho_g)\, dz$ | Volume $\propto 1/R$ | Links mass to expansion |
| Mixture density perturbation | $\delta\rho_m \approx -\rho_\ell \alpha$ | $\propto -m/(R\rho_g)$ | Drives pressure changes |
| Identifiability | Operator gain $\sim 1/R$ | Noise amplification $\sim R$ | Sets detection threshold |

**Table 8:** Surface observables and their dependence on the retardation factor.

| Model layer | Description | Primary use | Main limitation |
|---|---|---|---|
| Full drift-flux + dissolution | PDEs in $(p, T, \alpha, m_f, m_d)$ with finite-rate $\Gamma$ | Reference for detailed dynamics | Higher computational cost |
| Retarded transport model | Scalar $m$ with $u_{\text{eff}}$ and $R(z,t)$ | Fast prediction of migration and holdup | Relies on small-holdup assumptions |
| Similarity-law estimate | Closed-form $t_{\text{arr}}$ and scaling relations | Quick screening and bounding | Uses averaged parameters only |
| Constrained inversion layer | Deconvolution of influx from surface data with constraints | Reconstructs admissible influx histories | Ill-conditioned when $R$ is large |

**Table 9:** Hierarchy of modeling layers used for analysis, scaling, and inversion.

vertical segment. The mixture consists of a liquid drilling fluid and methane that may exist as a free gas phase and as dissolved mass in the liquid. The model uses a drift-flux kinematic closure to represent slip between phases while maintaining a compact momentum description.

Let $p(z,t)$ denote pressure, $T(z,t)$ denote temperature, and $v_m(z,t)$ denote mixture superficial velocity [10]. Let $\alpha(z,t)$ denote free-gas volume fraction, $\rho_g(p,T)$ denote gas density, and $\rho_\ell(p,T,c)$ denote liquid density, where $c(z,t)$ is dissolved methane concentration per unit liquid mass. The mixture density is $\rho_m = \alpha\rho_g + (1-\alpha)\rho_\ell$. The drift-flux closure relates phase velocities to mixture velocity through a drift term $V_d$,

$$v_g = v_m + V_d(\alpha, p, T, v_m; \eta), \quad v_\ell = v_m - \frac{\alpha}{1-\alpha} V_d(\alpha, p, T, v_m; \eta), \tag{2.1}$$

where $\eta$ denotes closure parameters capturing annular geometry and buoyant rise behavior. The conservative methane inventories are expressed most stably using masses per mixture volume [11]. Define free methane mass per mixture volume $m_f = \alpha\rho_g$ and dissolved methane mass per mixture volume $m_d = (1-\alpha)\rho_\ell c$, so total methane mass per mixture volume is $m = m_f + m_d$. With this choice, the dissolved state remains well scaled even when $(1-\alpha)$ varies, and the partitioning between $m_f$ and $m_d$ becomes an explicit relaxation mechanism rather than an algebraic switch.

The governing equations include mixture mass conservation, methane mass conservation for both inventories with interphase transfer, mixture momentum, and a reduced thermal balance. Mixture mass

conservation is

$$\frac{\partial}{\partial t}\left(A\rho_m\right) + \frac{\partial}{\partial z}\left(A\rho_m v_m\right) = 0. \tag{2.2}$$

The methane inventory balances are [12]

$$\frac{\partial}{\partial t}\left(Am_f\right) + \frac{\partial}{\partial z}\left(Am_f v_g\right) = -A\Gamma + As_{in}, \tag{2.3}$$

$$\frac{\partial}{\partial t}\left(Am_d\right) + \frac{\partial}{\partial z}\left(Am_d v_\ell\right) = A\Gamma, \tag{2.4}$$

where $\Gamma(z,t)$ is the net dissolution rate per mixture volume, positive for dissolution and negative for exsolution, and $s_{in}(z,t)$ is an influx source localized near $z = L$ or imposed as a boundary flux. The mixture momentum equation is written in a compressible mixture form,

$$\frac{\partial}{\partial t}\left(A\rho_m v_m\right) + \frac{\partial}{\partial z}\left(A\rho_m v_m^2\right) + A\frac{\partial p}{\partial z} = -A\rho_m g\cos\theta - A\Delta_w, \tag{2.5}$$

where $\Delta_w$ is an effective wall-shear contribution per mixture volume, modeled as a dissipative function of $v_m$ and state-dependent viscosity and density surrogates. Thermal coupling is represented by a reduced mixture energy balance,

$$\frac{\partial}{\partial t}\left(A\rho_m h_m\right) + \frac{\partial}{\partial z}\left(A\rho_m v_m h_m\right) = -Av_m\frac{\partial p}{\partial z} + Aq_{\text{wall}}(T, T_f; \kappa), \tag{2.6}$$

where $h_m$ is mixture specific enthalpy, $T_f(z)$ is an ambient profile, and $\kappa$ is an effective heat transfer parameter. The thermal model is retained because $\rho_g$ and equilibrium solubility depend on $T$, and because temperature variation can shift the exsolution depth and thus the onset of strong surface sensitivity [13].

The solubility mechanism is represented as a combination of an equilibrium capacity and finite-rate relaxation. Let $c^\star(p,T;\chi)$ denote the equilibrium dissolved concentration per unit liquid mass, parameterized by a small vector $\chi$ representing fluid composition effects. Define the equilibrium dissolved mass per mixture volume as

$$m_d^\star(p,T,\alpha) = (1-\alpha)\rho_\ell(p,T,c^\star(p,T;\chi))\,c^\star(p,T;\chi). \tag{2.7}$$

Finite-rate mass transfer is modeled as relaxation toward equilibrium, [14]

$$\Gamma = \lambda_m(\alpha,p,T,v_m)\left(m_d^\star(p,T,\alpha) - m_d\right), \quad \lambda_m \geq 0, \tag{2.8}$$

where $\lambda_m$ is an effective relaxation rate that can depend on interfacial area and circulation. This form ensures that $\Gamma(m_d - m_d^\star) \leq 0$, so mass transfer reduces disequilibrium. It also yields two important limits: a fast-equilibrium regime where $\lambda_m$ is large and $m_d \approx m_d^\star$, and a slow-transfer regime where disequilibrium persists and partitioning introduces an additional delay mechanism beyond equilibrium capacity.

Non-dimensionalization is used to expose the controlling groups that determine retardation and observability. Let $L$ be the characteristic length, let $U$ be a characteristic transport velocity scale, and let $P$ be a characteristic pressure scale, with $U$ chosen as a typical mixture velocity under circulation or a typical drift velocity under non-circulating conditions [15]. Define dimensionless variables

$$\tilde{z} = \frac{z}{L}, \quad \tilde{t} = \frac{U}{L}t, \quad \tilde{v}_m = \frac{v_m}{U}, \quad \tilde{V}_d = \frac{V_d}{U}, \quad \tilde{p} = \frac{p}{P}, \quad \tilde{T} = \frac{T}{T_0}, \tag{2.9}$$

and scale methane masses by a characteristic methane mass density $M_0$, setting $\tilde{m}_f = m_f/M_0$, $\tilde{m}_d = m_d/M_0$, and $\tilde{m} = \tilde{m}_f + \tilde{m}_d$. Define a dimensionless relaxation Damköhler number

$$\mathrm{Da}_m = \frac{\lambda_{m,0} L}{U}, \tag{2.10}$$

where $\lambda_{m,0}$ is a representative relaxation rate. Define a dimensionless solubility capacity ratio, which plays the role of a retardation parameter, by comparing the equilibrium dissolved mass capacity to free gas mass scale at relevant conditions. A practical choice is

$$\mathcal{S}(\tilde{p}, \tilde{T}) = \frac{\rho_{\ell,0}\, c^\star(p,T)}{\rho_g(p,T)}, \tag{2.11}$$

which measures how much methane mass per mixture volume can be stored dissolved relative to the mass per mixture volume of a unit holdup free gas phase at the same $(p,T)$ [16]. In regimes where $\mathcal{S}$ is large, dissolution capacity is high and free gas is strongly buffered; in regimes where $\mathcal{S}$ is small, the dissolved inventory is limited and free gas dominates.

These groups appear directly in reduced forms of the methane transport equations. Summing the methane inventory balances yields conservation of total methane mass,

$$\frac{\partial}{\partial t}\,(Am) + \frac{\partial}{\partial z}\left(A(m_f v_g + m_d v_\ell)\right) = A s_{in}. \tag{2.12}$$

The flux is a weighted mixture of gas and liquid velocities. In regimes where methane mass is mostly dissolved, the flux is close to liquid advection; in regimes where methane mass is mostly free, the flux includes drift [17]. The goal of the subsequent sections is to reduce this flux into a retarded drift form where the dissolved inventory enters as a multiplicative retardation factor on effective methane propagation, analogous to how sorption retards solute transport.

## 3. Retardation Limits and Effective Compressibility

The key mechanism to be isolated is the buffering effect of dissolved methane on free-gas emergence. This section derives reduced equations in two regimes that are often relevant for operational interpretation: a fast-equilibrium regime where mass transfer is rapid relative to axial transport, and an intermediate regime where mass transfer is finite but still sufficiently strong to justify a perturbation approach. In both regimes, the dissolved inventory induces an effective retardation factor that slows the propagation of methane mass relative to free-gas holdup and therefore weakens early surface sensitivity.

In the fast-equilibrium limit $\mathrm{Da}_m \gg 1$, the relaxation term forces $m_d \approx m_d^\star(p,T,\alpha)$ in leading order, except in thin boundary layers in time or space near sudden changes. In this limit, total methane mass $m = m_f + m_d$ is the conserved transported quantity, and the partition $m_f = m - m_d^\star$ follows the moving equilibrium capacity [18]. The methane dynamics can therefore be expressed as a single transport equation for $m$, coupled to an algebraic relation determining $m_f$ from $m$ and state. To obtain a tractable form, consider the common regime in which holdup is small early, so $\alpha \ll 1$ and $1-\alpha \approx 1$. Then $m_d^\star$ is approximately independent of $\alpha$ in leading order, and one can write $m_d^\star \approx \rho_\ell(p,T,c^\star)\, c^\star(p,T)$. Under these assumptions, free methane mass becomes

$$m_f \approx \max\!\big(0,\; m - \rho_\ell(p,T,c^\star)\, c^\star(p,T)\big), \tag{3.1}$$

where the max reflects that when total methane mass is below the dissolved capacity, free methane can be negligible [19]. This representation captures the buffering regime: methane mass can increase without producing free gas until it exceeds dissolved capacity at the local $(p,T)$.

A more informative reduction arises by linearizing around a regime where free methane is present but small, so that $m_f$ is nonzero but $m_d$ still represents a substantial fraction of total mass. In this regime, $m_d$

changes with $m$ through equilibrium partitioning. Differentiating the equilibrium relation yields a local relation between changes in total methane and changes in free methane [20]. Let $m_d^\star(p,T)$ be treated as a capacity term independent of $m$ at fixed $(p,T)$, then $\partial m_f/\partial m \approx 1$ when free methane is present. This does not yield retardation. Retardation emerges when the equilibrium dissolved mass depends on pressure and when pressure itself responds to methane addition through hydrostatic and compressibility effects, and when finite-rate transfer introduces a dynamic lag in $m_d$ relative to $m_d^\star$. The leading-order equilibrium alone changes the threshold for free gas appearance, but the dynamic buffering that slows propagation emerges from the combination of equilibrium capacity and finite transport.

To extract a clean retardation factor, consider an intermediate regime in which methane remains in two forms along the ascent path, and the dissolved concentration remains close to equilibrium but not identical, so that $m_d = m_d^\star - \epsilon\delta$ with small $\epsilon$ proportional to $1/\mathrm{Da}_m$. Substitute into the dissolved inventory balance and retain leading-order terms [21]. In a simplified geometry with slowly varying $A$ and with $v_m$ and $V_d$ treated as given functions of depth and time, one obtains a relaxation-advection equation for the disequilibrium $\delta$, which in turn modifies the relationship between $m_f$ and $m$. Eliminating $\delta$ yields a retarded transport equation for $m$ in which the effective methane flux depends on an effective velocity that is reduced by a factor that depends on solubility capacity and on relaxation rate.

A more transparent derivation uses an analogy to linear sorption. Suppose that, over a time window of interest, the equilibrium dissolved mass can be linearized with respect to total methane mass through an effective partition coefficient, which is reasonable if changes in total methane remain within a regime where $c^\star(p,T)$ varies slowly relative to methane mass variation and where the liquid remains far from saturation limits. Represent this as [22]

$$m_d \approx K(p,T)\, m_f, \quad K \geq 0, \tag{3.2}$$

so that $m = m_f + m_d \approx (1+K)m_f$. In this representation, $K$ is an effective capacity ratio that can be related to $\mathcal{S}$ and to the relative volumes of phases. If $K$ is large, a small amount of free methane corresponds to a large dissolved inventory, meaning that free gas is strongly buffered. The key consequence is that the methane mass that is actually advected by the drift velocity is the free methane component, while the dissolved component is advected with the liquid. Therefore, the methane flux can be approximated as

$$m_f v_g + m_d v_\ell \approx m_f(v_m + V_d) + K m_f \left(v_m - \frac{\alpha}{1-\alpha} V_d\right). \tag{3.3}$$

In the small holdup regime $\alpha \ll 1$, the slip correction in $v_\ell$ is negligible, and the flux becomes [23]

$$m_f v_g + m_d v_\ell \approx (1+K)\, m_f v_m + m_f V_d. \tag{3.4}$$

Using $m \approx (1+K)m_f$ yields

$$m_f v_g + m_d v_\ell \approx m v_m + \frac{m}{1+K} V_d. \tag{3.5}$$

Thus the methane mass behaves as if it were advected by the mixture velocity plus a reduced drift component $V_d/(1+K)$. The factor

$$R = 1 + K \tag{3.6}$$

plays the role of a retardation factor [24]. In this leading-order approximation, the effective velocity of methane mass relative to the liquid is reduced by $R$, so methane mass migrates upward more slowly than free gas would if it were entirely in the gas phase. This result is not a claim about the detailed bubble kinematics; it is a statement about how dissolution redistributes methane mass into a phase that does not experience the same buoyant drift, producing a macroscopic slowing of the methane mass front.

The same factor $R$ also changes the mapping from methane mass to free-gas holdup. Since $m_f \approx m/R$ in this regime, the holdup becomes

$$\alpha = \frac{m_f}{\rho_g(p,T)} \approx \frac{m}{R\,\rho_g(p,T)}. \tag{3.7}$$

Therefore, for a given total methane mass per mixture volume, the free-gas holdup and thus the hydrostatic perturbation are reduced by $1/R$ [25]. This yields an effective compressibility interpretation. Many surface indicators respond primarily to free-gas holdup because holdup changes mixture density and pressure gradients. Dissolution therefore reduces the sensitivity of these indicators to total methane mass by the same factor that retards the methane drift. The implication is that early detection, which depends on small changes in surface signals, is inherently weakened by large $R$.

The retardation factor can be connected to equilibrium solubility capacity and fluid properties [26]. A simple relation is obtained by approximating $K$ as the ratio of equilibrium dissolved methane mass per mixture volume to free methane mass per mixture volume at the same conditions. In the small holdup regime, $m_f = \alpha\rho_g$ and $m_d \approx \rho_\ell c$. If the dissolved concentration remains near equilibrium and is proportional to the amount of methane available, then $K$ scales like $\rho_\ell c^\star/(\rho_g \alpha)$, which is large for small $\alpha$. For macroscopic behavior, however, one seeks a $K$ that is independent of $\alpha$ and instead captures how changes in methane mass allocate between inventories [27]. A practical estimate is that, locally, a small increment $\delta m$ in total methane allocates fraction $\phi$ to free gas and $(1-\phi)$ to dissolved gas, so that $K = (1-\phi)/\phi$. The fraction $\phi$ depends on proximity to saturation and on kinetics, but it can be bounded using solubility capacity $\mathcal{S}$ and total methane concentration. This yields bounded retarded velocities rather than singular behavior as $\alpha \to 0$.

The finite-rate case modifies the above equilibrium-based relation by making $K$ history dependent. When relaxation is slow, methane can remain free longer, effectively reducing $K$ and reducing retardation. When relaxation is fast, $K$ approaches its equilibrium value [28]. A simple dynamic generalization models $K$ as a first-order filter driven by equilibrium capacity, yielding an effective retardation that is time varying. This perspective is useful because it separates two operationally distinct effects: equilibrium capacity sets how much methane can be stored dissolved at a given $(p,T)$, while kinetics sets how quickly that storage is realized. Both contribute to early ambiguity. The analysis later uses this structure to derive observability limits and to motivate inversion operators that treat $R$ as uncertain but bounded.

## 4. Similarity Laws for Migration and Arrival Time Across Circulation Regimes

The retardation theory yields a compact expression for methane transport in terms of an effective velocity [29]. This section uses that expression to derive similarity laws for methane migration and arrival time under two limiting operational regimes: non-circulating conditions where drift dominates, and circulating conditions where mixture advection dominates but slip remains relevant. The aim is not to generate a single closed-form solution for all conditions, but to derive scaling relations that can be evaluated quickly and that make the dependence on solubility and circulation explicit.

Assume, for the purpose of deriving similarity laws, that the annulus area is approximately constant and that the drift velocity can be represented by a characteristic value $V_b$ for the relevant holdup regime. Under small holdup and weak area variation, the retarded methane transport equation derived previously can be approximated as a scalar conservation law for the methane mass per mixture volume $m$: [30]

$$\frac{\partial m}{\partial t} + \frac{\partial}{\partial z}\left(m v_m + \frac{m}{R} V_b\right) = s_{in}(z,t), \tag{4.1}$$

with $R \geq 1$ representing the retardation factor. In the simplest case of a localized influx at the bottom, $s_{in}$ is nonzero only near $z = L$ or enters as a boundary flux. The equation is linear in $m$ when $v_m$, $V_b$, and $R$ are treated as given, so one can derive closed-form expressions for arrival times and for the evolution of integrated methane mass.

In a non-circulating regime, $v_m \approx 0$ and transport is dominated by the drift term. The effective methane propagation velocity is $V_b/R$, so a methane mass front generated at $z = L$ reaches the wellhead after a time

$$t_{\text{arr}}^{(0)} \approx \frac{L}{V_b/R} = \frac{R\,L}{V_b}. \tag{4.2}$$

This scaling states that dissolution lengthens the methane mass arrival time by a factor $R$ relative to the free-gas drift time [31]. The same scaling implies that, even if a small amount of free gas migrates faster, the methane mass that can later exsolve near the surface is delayed in proportion to the amount stored dissolved. This provides a mechanistic explanation for why soluble kicks can present weak early indicators yet still lead to later rapid unloading, because a large methane mass can be advected upward slowly and then appear rapidly as free gas near the surface when pressure falls.

In a circulating regime with nonzero mixture velocity, the effective methane velocity becomes $v_m + V_b/R$ when flow is upward. If $v_m$ is large compared with $V_b/R$, then methane transport is dominated by advection, and retardation affects primarily the partitioning and thus the magnitude of free-gas indicators rather than the arrival time. The leading-order arrival time scaling becomes [32]

$$t_{\text{arr}}^{(\text{circ})} \approx \frac{L}{\bar{v}_m + \bar{V}_b/R}, \tag{4.3}$$

where overbars denote representative averages along the path. This expression makes explicit a transition between a drift-dominated regime and an advection-dominated regime. In drift-dominated regimes, $t_{\text{arr}}$ scales like $R$. In advection-dominated regimes, $t_{\text{arr}}$ is relatively insensitive to $R$ because $\bar{v}_m$ dominates, but $R$ still reduces free-gas holdup and therefore reduces surface sensitivity, affecting detectability even if arrival time is similar.

The above expressions can be generalized to depth-dependent velocities and retardation by integrating along characteristics. If $v_m(z,t)$ and $V_b(z,t)$ vary slowly in time, then the characteristic for methane mass satisfies

$$\frac{dz}{dt} = v_m(z,t) + \frac{1}{R(z,t)} V_b(z,t). \tag{4.4}$$

The arrival time is then the solution of [33]

$$\int_0^{t_{\text{arr}}} \left( v_m(z(t),t) + \frac{V_b(z(t),t)}{R(z(t),t)} \right) dt = L, \quad z(0) = L, \quad z(t_{\text{arr}}) = 0. \tag{4.5}$$

In practice, for real-time use, this integral can be approximated by assuming $v_m$ is set by pump rate and $V_b$ by a buoyancy scaling based on annulus geometry, and by using a representative $R$ computed from $(p,T)$ near the bottom or along the path. The value of the theory is that it provides a transparent place to introduce solubility effects: they enter only through $R$ and through the mapping from $m$ to free-gas holdup, not through ad hoc modifications of drift correlations.

Similarity laws also apply to the evolution of surface indicators. For example, pit gain is driven by the net volumetric expansion of free gas near the surface and by return flow imbalance [34]. Since free-gas holdup is reduced by $1/R$ for a given methane mass, early pit gain scales similarly. Under small holdup and linearized hydraulics, pit gain rate can be approximated as proportional to the time derivative of integrated free gas volume in the annulus. If $M(t) = \int_0^L A m\, dz$ is total methane mass in the annulus and if a fraction $1/R$ appears as free methane mass, then the free gas volume is approximately $V_g(t) \approx \int_0^L A\alpha\, dz \approx \int_0^L A \frac{m}{R\rho_g}\, dz$. Therefore, for a given methane mass influx history, pit gain signals scale inversely with $R$ until exsolution changes the partition rapidly near the surface.

The analysis also yields a natural dimensionless grouping for operational regime classification. Define a circulation number [35]

$$C = \frac{\bar{v}_m}{\bar{V}_b/R} = \frac{R\,\bar{v}_m}{\bar{V}_b}. \tag{4.6}$$

When $C \ll 1$, drift dominates methane transport and retardation strongly affects arrival time. When $C \gg 1$, advection dominates transport and retardation affects primarily indicator amplitude and internal inventory rather than arrival time. This grouping clarifies that increasing circulation can shorten the time to surface manifestation even under strong dissolution, but it may also change the thermodynamic path of methane, potentially moving dissolved inventory into lower-pressure regions faster and thereby accelerating exsolution near the surface. The present paper does not treat that acceleration as a separate mechanism; it is already implied by the fact that $R$ depends on $(p, T)$ and therefore varies along the path.

A further similarity law concerns the onset of exsolution in upper sections. If the dissolved inventory is near equilibrium at depth and pressure decreases along the ascent path, the equilibrium capacity decreases, and exsolution occurs when the local methane mass exceeds capacity. In the fast-equilibrium limit, this onset is determined by the condition $m(z,t) \gtrsim m_d^\star(p(z,t), T(z,t))$ [36]. Because $m$ is transported along characteristics and $m_d^\star$ is a function of pressure and temperature, one can define an exsolution depth $z_e(t)$ implicitly by

$$m(z_e(t), t) = m_d^\star(p(z_e(t), t), T(z_e(t), t)). \tag{4.7}$$

Above this depth, a portion of methane must appear as free gas, and surface sensitivity increases. This provides a mechanism-based explanation for a common qualitative pattern: long periods of weak surface response followed by rapid changes when the exsolution front approaches the surface. In the retarded transport description, this behavior is controlled by the interplay between the methane mass profile $m(z,t)$ and the equilibrium capacity profile $m_d^\star(p(z,t), T(z,t))$, both of which can be estimated or bounded in real time [37].

## 5. Surface Observables and Constrained Inversion of Influx History

Similarity laws provide timing and scaling insight, but operational monitoring requires mapping between surface measurements and the underlying influx history. This section develops a constrained inversion framework grounded in the retarded transport theory. The framework is designed to clarify which aspects of influx can be inferred from surface pressure and pit gain, and how solubility buffering limits early inference by reducing sensitivity.

Let the available measurements be wellhead pressure $p_w(t) = p(0,t)$ and pit volume $V_{\mathrm{pit}}(t)$ or pit gain rate $\dot{V}_{\mathrm{pit}}(t)$, with known pump rate and choke setting entering as inputs. The observation operator mapping downhole state to measurements is nonlinear, but in early stages where holdup is small, a linearized mapping can be derived. The purpose of the linearized mapping is not to provide a complete predictor, but to provide an inversion operator for the methane mass flux or for its bounds [38].

Under small holdup, the dominant effect of methane on the pressure field is through a reduction in mixture density, which reduces hydrostatic head. Linearize mixture density around the liquid-only state. Write $\rho_m \approx \rho_\ell - \alpha(\rho_\ell - \rho_g)$, and since $\rho_\ell \gg \rho_g$ at most depths, $\rho_m \approx \rho_\ell(1-\alpha)$ in leading order. The hydrostatic pressure at depth $z$ is then

$$p(z,t) \approx p_w(t) + \int_0^z \rho_\ell(\zeta,t) g \cos\theta(\zeta)\, d\zeta - \int_0^z \rho_\ell(\zeta,t)\alpha(\zeta,t) g \cos\theta(\zeta)\, d\zeta + \text{friction terms}. \tag{5.1}$$

The perturbation in wellhead pressure relative to a baseline can therefore be related to the integral of holdup weighted by hydrostatic coefficient and to frictional changes [39]. In early time, friction changes

due to small holdup can be treated as second order, leaving a leading-order relation

$$\delta p_w(t) \approx -\int_0^L w_p(\zeta)\,\alpha(\zeta,t)\,d\zeta + \delta p_{\mathrm{op}}(t), \quad w_p(\zeta) = \rho_\ell(\zeta) g \cos\theta(\zeta), \tag{5.2}$$

where $\delta p_{\mathrm{op}}$ aggregates operational pressure variations due to pump and choke inputs that can be estimated or filtered using known inputs. Substituting the retardation relation $\alpha \approx m/(R\rho_g)$ yields

$$\delta p_w(t) \approx -\int_0^L w_p(\zeta)\,\frac{m(\zeta,t)}{R(\zeta,t)\rho_g(\zeta,t)}\,d\zeta + \delta p_{\mathrm{op}}(t). \tag{5.3}$$

This expression makes the buffering effect explicit: for a fixed methane mass distribution $m(\zeta,t)$, the wellhead pressure perturbation is reduced by $1/R$. Therefore, early-time pressure-based detection is weakened when $R$ is large.

Pit gain is driven by volumetric expansion and by return flow imbalance [40]. In a simplified model where tank dynamics are neglected, pit volume change is the integral of net surface flow imbalance,

$$\dot{V}_{\mathrm{pit}}(t) = Q_{\mathrm{in}}(t) - Q_{\mathrm{out}}(t) + \omega(t), \tag{5.4}$$

where $\omega$ aggregates sensor noise and unmodeled tank effects. The outflow $Q_{\mathrm{out}}$ depends on mixture density and compressibility in the return line and at the surface. In early stages, a useful approximation relates pit gain to the rate of change of free gas volume in the annulus, because gas expansion increases return flow volume relative to pump inflow. If $V_g(t) = \int_0^L A\alpha\,dz$ is free gas volume, a linearized relation of the form $\dot{V}_{\mathrm{pit}} \approx \dot{V}_g$ can be used as an interpretive proxy, acknowledging that operational conditions and surface separation can modify this mapping. Substituting $\alpha \approx m/(R\rho_g)$ yields [41]

$$V_g(t) \approx \int_0^L A(z)\,\frac{m(z,t)}{R(z,t)\rho_g(z,t)}\,dz. \tag{5.5}$$

Thus both wellhead pressure and pit gain depend on the same weighted integral of $m/R$, implying that they can be redundant in early time unless additional information, such as frictional signature differences or temperature measurements, is used. This redundancy is one reason early inference is ambiguous: two different methane mass distributions can yield similar integrals, especially when $R$ is uncertain.

The inversion problem can be posed as reconstructing the influx mass rate $\dot{m}_{in}(t)$ from measurements. In the retarded transport approximation with known effective velocity, $m$ is governed by a linear transport equation, so $m$ is a linear functional of $\dot{m}_{in}$. Therefore, measurements can be written as a convolution-like relation between $\dot{m}_{in}$ and observed signals. The simplest case assumes constant effective velocity $u_{\mathrm{eff}} = v_m + V_b/R$ and negligible operational perturbations. Then a boundary influx at $z = L$ produces a methane mass distribution that is a translated and scaled version of the influx history. The resulting wellhead pressure perturbation is approximately a filtered and delayed version of $\dot{m}_{in}$, with delay $t_{\mathrm{arr}}$ and gain proportional to $1/R$. This motivates a deconvolution approach.

To formulate a stable constrained inversion, represent the influx rate as a nonnegative function $q(t)$ in appropriate units [42]. The forward mapping to a measurement $y(t)$, representing a combined indicator after removing operational baseline, can be written abstractly as

$$y(t) = \int_0^t k(t-\tau; R, \Theta)\,q(\tau)\,d\tau + \epsilon(t), \tag{5.6}$$

where $k$ is an impulse response determined by transport velocity, gas density variation, weighting functions in the measurement, and parameters $\Theta$ including drift and geometry effects, and $\epsilon$ is measurement noise and residual modeling error. The presence of $R$ in $k$ emphasizes that solubility buffering scales the

gain and can broaden the kernel by delaying free gas emergence. The inversion seeks $q(t) \geq 0$ that minimizes measurement mismatch subject to smoothness or bounded variation priors that reflect plausible influx behavior. A suitable constrained functional is [43]

$$\min_{q \geq 0} \quad \int_0^T \left( y(t) - \int_0^t k(t-\tau)\, q(\tau)\, d\tau \right)^2 dt + \lambda \int_0^T \left( \frac{dq}{dt} \right)^2 dt, \tag{5.7}$$

where $T$ is the window length and $\lambda$ controls regularization. The positivity constraint prevents unphysical negative influx that could otherwise be used to fit noise, which is especially important when $R$ reduces sensitivity and makes the inversion ill-conditioned early.

The ill-conditioning induced by large $R$ can be quantified through operator norms. The effective gain of the forward operator scales like $1/R$, so the inverse operator norm scales like $R$ in leading order, meaning that noise amplification grows with dissolution capacity [44]. This yields an identifiability bound: for a given measurement noise level, there exists a minimum detectable influx magnitude that scales with $R$. In practice, this implies that early detection thresholds should be adjusted for solubility buffering, and that ignoring buffering can lead to overconfident conclusions in both directions, either dismissing a real influx because the signal is weak or overestimating influx because the signal is delayed and then rises rapidly.

A thermodynamic mechanism further complicates inversion because $R$ is not constant; it depends on $p$ and $T$. Therefore, inversion should treat $R$ as uncertain and possibly time varying. A conservative approach is to bound $R$ within an interval $[R^-, R^+]$ computed from bounds on $c^\star(p,T)$ and on liquid density and to produce a set of feasible influx histories consistent with measurements for all $R$ in that interval [45]. This yields an interval-valued inference rather than a point estimate. The practical benefit is that it produces an early-time ambiguity band that can be communicated to decision logic without hiding uncertainty. The theory of this paper supports such bounding because the forward operator depends on $R$ primarily through scaling and through effective velocity, so bounds on $R$ translate into bounds on both delay and gain.

An important implication of the inversion structure is that adding information that affects $R$ can reduce ambiguity. For example, temperature measurements constrain $c^\star(p,T)$ and thus $R$, and downhole pressure measurements constrain $p$ and thus both $R$ and gas density [46]. Conversely, if only surface measurements are available, $R$ can be confounded with influx magnitude and with drift velocity, implying that early-time influx sizing is intrinsically uncertain. This is not an algorithm failure; it is an information limitation imposed by dissolution buffering. The subsequent section discusses how this limitation can be addressed by bounding and by using similarity laws to compute conservative timelines, rather than by insisting on precise early estimates.

## 6. Numerical Illustration Strategy and Discussion of Regime Validity

A theory intended for operational interpretation must be accompanied by a clear strategy for numerical illustration and for assessing regime validity [47]. The present work is analytic and reduction-oriented, so the numerical role is to test the extent to which the retarded transport approximation reproduces the qualitative and quantitative behavior of a more complete drift-flux model with finite-rate dissolution and realistic pressure and temperature variation. Because the aim is not to report a specific field calibration, numerical illustrations are framed as representative studies designed to stress the mechanisms that the theory claims to capture.

A suitable numerical illustration compares three model layers. The first layer is a baseline drift-flux annular model with explicit dissolved inventory and finite-rate relaxation, discretized in space and integrated implicitly where needed for stiffness. The second layer is a reduced retarded transport model for total methane mass $m$ with an effective velocity $v_m + V_b/R$ and an algebraic relation for holdup $\alpha \approx m/(R\rho_g)$ [48]. The third layer is a further reduced similarity-law estimate that predicts arrival time and indicator scaling using averaged parameters. Agreement among these layers can be evaluated in

terms of arrival time, onset of exsolution near the surface, and early-time scaling of wellhead pressure perturbation magnitude.

The retarded transport approximation is expected to be most accurate in regimes where holdup remains small over most of the annulus and where the drift velocity can be approximated by a weakly varying function. In such regimes, transport is dominated by advection and buoyant slip, and the primary nonlinearities come from gas density variation and from solubility capacity variation. The theory captures these through $\rho_g(p,T)$ and through $R(p,T)$ [49]. In contrast, when holdup becomes large and flow transitions out of bubbly regimes, drift-flux closures and friction models can change qualitatively, and the effective partition between dissolved and free methane can interact strongly with flow regime. In such cases, the retarded transport model remains a useful interpretive bound but should not be treated as a precise predictor.

Finite-rate dissolution introduces additional time scales. When $\mathrm{Da}_m$ is moderate, disequilibrium can persist, and the effective retardation factor becomes time dependent. The retarded transport theory can accommodate this by treating $R$ as a dynamic state or by bounding it between an equilibrium value and a kinetic-limited value. For example, if dissolution is slow, $K$ is smaller and $R$ is closer to one, implying weaker retardation and stronger early free-gas signals [50]. As circulation increases, mass transfer can become faster, increasing $R$ and thus increasing buffering. This interaction between circulation and buffering is not paradoxical; it reflects that circulation both advects methane upward and enhances dissolution kinetics, so it can reduce arrival time while also reducing early holdup signals.

The pressure and temperature dependence of $R$ introduces another regime consideration. At high pressure, solubility capacity is often higher, so $R$ can be large, making early signals weak [51]. As methane migrates upward and pressure decreases, $R$ can decrease, and exsolution can occur. Therefore, the buffering effect is inherently nonuniform along the annulus. The retarded transport model accounts for this by allowing $R(z,t)$ to vary, but similarity laws often use a representative $R$ for timing. A useful practice is to use $R$ near the bottom for early detectability bounds and to use a path-average $R$ for arrival time estimates. This yields conservative estimates: bottom $R$ often overestimates buffering early, producing conservative detection thresholds, while path-average $R$ yields reasonable arrival time scaling [52].

The presence of operational disturbances such as pump ramps and choke changes introduces an additional issue: separating influx-driven signals from operational transients. The retarded transport theory does not replace operational filtering; it provides structure for how methane mass affects signals. In a numerical illustration, operational inputs should be included explicitly and their effect on baseline pressure should be subtracted or modeled so that the residual signal can be attributed to methane. This is essential because solubility buffering reduces methane signal-to-noise ratio early, making baseline removal a dominant source of error. Therefore, the practical use of the theory is to supply a physically constrained mapping from methane mass to residual signals, while operational filtering supplies the baseline [53].

The theory also clarifies why mechanistic solubility models matter even when the transport model is reduced. In particular, the mapping $R(p,T)$ depends on the equilibrium solubility map $c^\star(p,T)$ and on liquid swelling behavior, both of which can be uncertain in synthetic oil-based systems. Rather than treating these as nuisance, the present theory treats them as the primary levers that set early observability. This is consistent with the existence of mechanistic riser models that have explicitly modeled methane dissolution and compared against thermodynamic benchmarks [54]. Manikonda et al. (2020) [55] presented a state-of-the-art mechanistic framework for predicting how gas kicks evolve in a riser with synthetic-based drilling fluid, explicitly predicting methane solubility and reporting that methane liquid-phase mole fraction estimates agreed with an external process simulator with a maximum 8% deviation while also matching bubble-point location estimates, indicating that thermodynamic partitioning in synthetic oil-based systems can be modeled in a compact mechanistic form rather than being relegated to purely empirical delays. In the context of the present paper, this supports the assumption that $R(p,T)$ can be bounded or calibrated in a principled way, enabling the retardation theory to produce operationally meaningful bounds.

Finally, it is important to articulate what the theory is intended to provide. It is intended to provide scaling relations and inversion operators that are structurally consistent with conservation and solubility buffering. It is not intended to serve as a universal forward simulator across all regimes [56]. Its value is highest where early interpretation is most ambiguous, because it provides a way to quantify ambiguity and to produce conservative bounds on methane mass and on arrival timelines, rather than relying on heuristic delays or assuming insolubility. In real-time systems, such bounds can inform whether muted early signals can be safely dismissed or whether a latent dissolved inventory remains plausible and therefore requires caution.

## 7. Conclusion

This paper developed a retardation-based theory for soluble methane kicks in synthetic and oil-based drilling fluids by deriving reduced transport and observation relations that explicitly represent dissolved inventory as a dynamic buffer. Starting from a drift-flux annular model with free and dissolved methane inventories and finite-rate relaxation toward an equilibrium solubility capacity, the analysis identified a retardation factor that reduces the effective buoyant drift component of methane transport and simultaneously weakens the mapping from total methane mass to free-gas holdup. This factor yields closed-form similarity laws for ascent time and clarifies how circulation changes shift the system between drift-dominated and advection-dominated regimes while preserving the buffering effect on early detectability [57]. A linearized surface-signature mapping was derived that relates wellhead pressure and pit gain to weighted integrals of retarded methane mass, making explicit the mechanism by which dissolution reduces signal-to-noise ratio and increases ill-conditioning of early-time inversion. A constrained deconvolution formulation was then presented to reconstruct admissible influx histories from surface measurements under positivity and smoothness constraints, with a natural pathway to uncertainty bounds through interval-valued retardation factors.

The broader implication is that solubility buffering should be treated as a first-order mechanism in early-time interpretation because it changes both the timeline of migration and the sensitivity of surface observables to underlying methane mass. The theory offers a compact analytic layer that can complement detailed simulators by providing scaling laws, detectability bounds, and physically constrained inversion operators that remain valid across non-circulating and circulating regimes under HPHT conditions. Future work can extend the retardation framework to explicitly incorporate strong holdup regimes through regime-dependent drift and friction bounds, incorporate richer thermal coupling to refine exsolution-front prediction, and integrate bounded-uncertainty formulations so that real-time monitoring can report conservative methane inventory envelopes rather than single-valued estimates in intrinsically ambiguous soluble regimes [58].

## References

[1] J. Grow, J. Miller, C. Mull, and K. J. Bird, "Seismic stratigraphy near the tunalik well, north slope, alaska," *AAPG Bulletin*, vol. 79, 4 1995.

[2] Q. Chou, M. Murtaza, E. Mammadov, and R. Snyders-Blok, "Arctic drilling hazard identification relating to salt tectonics," in *Arctic Technology Conference*, OTC, 10 2016.

[3] D. Vavik, S. Sangesland, and M. Shayegh, "Loss of circulation an indication of hydrocarbon influx," in *SPE/IADC Managed Pressure Drilling and Underbalanced Operations Conference and Exhibition*, SPE, 4 2016.

[4] A. K. Sleiti, G. Takalkar, M. H. El-Naas, A. R. Hasan, and M. A. Rahman, "Early gas kick detection in vertical wells via transient multiphase flow modelling: A review," *Journal of Natural Gas Science and Engineering*, vol. 80, p. 103391, 2020.

[5] T. Bayer, B. V. Cunning, R. Selyanchyn, M. Nishihara, S. Fujikawa, K. Sasaki, and S. M. Lyth, "Proton conduction in nanocellulose - paper fuel cells," *ECS Meeting Abstracts*, vol. MA2016-02, pp. 2603–2603, 9 2016.

[6] R. A. Shishavan, C. Hubbell, H. D. Perez, J. D. Hedengren, D. S. Pixton, and A. P. Pink, "Multivariate control for managed-pressure-drilling systems by use of high-speed telemetry," *SPE Journal*, vol. 21, pp. 459–470, 4 2016.

[7] K. Bybee, "Analysis of alternative well-control methods for dual-density deepwater drilling," *Journal of Petroleum Technology*, vol. 59, pp. 61–63, 1 2007.

[8] K. Manikonda, A. R. Hasan, O. Kaldirim, J. J. Schubert, and M. A. Rahman, "Understanding gas kick behavior in water and oil-based drilling fluids," in *SPE Kuwait oil and gas show and conference*, p. D043S023R001, SPE, 2019.

[9] K. Kinik, F. Gumus, and N. Osayande, "A case study: First field application of fully automated kick detection and control by mpd system in western canada," in *SPE/IADC Managed Pressure Drilling & Underbalanced Operations Conference & Exhibition*, SPE, 4 2014.

[10] J. Feng, J. Fu, P. Chen, and L. Xu, "Investigation of methane/drilling mud phase behavior and its influence to hydrocarbon drilling activity," *Energy Science & Engineering*, vol. 7, pp. 1280–1291, 4 2019.

[11] K. Karahasan, J. S. Oyovwevotu, and W. E. S. Vielma, "Implementation of dispersed gas model for kick tolerance analysis of an hpht exploration well in norway," in *Abu Dhabi International Petroleum Exhibition & Conference*, SPE, 11 2017.

[12] S. G. Kreknin, K. Pushnikov, M. N. Makarevich, K. Burdin, V. Pivovarov, B. Kuzichev, M. Novikov, and K. Ronzhin, "Coiled tubing complex implementation at stimulation and testing project of deviated exploration gas well at chayandinskoe oilfield, yakutia, russia," in *SPE Russian Petroleum Technology Conference and Exhibition*, SPE, 10 2016.

[13] P. Oudeman, "Analysis of surface and wellbore hydraulics provides key to efficient blowout control," *SPE Annual Technical Conference and Exhibition*, 10 1996.

[14] R. Kiran, S. A. Naqavi, S. Salehi, and C. Teodoriu, "Human factors and non-technical skills: Towards an immersive simulation-based training framework for offshore drilling operations," in *SPE Annual Technical Conference and Exhibition*, SPE, 9 2019.

[15] F. R. Kodong, H. Sofyan, and H. Prapcoyo, "Implementasi aplikasi android-based untuk penanggulangan well kick pada pemboran minyak dan gas bumi," 12 2020.

[16] N. Kim, "Study of the pvt behavior of methane and ester-based drilling fluid mixtures," in *SPE Annual Technical Conference and Exhibition*, SPE, 9 2010.

[17] T. Jacobs, "Innovators seek to transform flaring into money and power," *Journal of Petroleum Technology*, vol. 72, pp. 24–29, 3 2020.

[18] E. Messana, "Data acquisition and recording system," in *Offshore Technology Conference*, OTC, 4 1979.

[19] H. Santos, E. Catak, and S. Valluri, "Kick tolerance misconceptions and consequences to well design," *SPE/IADC Drilling Conference and Exhibition*, 3 2011.

[20] A. Adams and S. Glover, "An investigation into the application of qra in casing design," in *SPE Applied Technology Workshop on Risk Based Design of Well Casing and Tubing*, SPE, 5 1998.

[21] J.-P. Hurel and C. van der Linden, "Matterhorn project," in *Offshore Technology Conference*, OTC, 5 2004.

[22] R. V. Rachapudi, S. M. Al-Nuimi, M. H. Q. Subaihi, T. C. Emegano, A. Elbekshi, G. Aydinoglu, M. Alyammahi, D. Gutierrez, and S. M. Abdelrehim, "Green field precommissioning challenges & capex optimization in view of global hostile oil economic environment - case study from middle east field," in *Abu Dhabi International Petroleum Exhibition & Conference*, SPE, 11 2019.

[23] D. A. Kornreich and R. V. E. Lovelace, "Dynamics of kicked and accelerated massive black holes in galaxies," 1 2008.

[24] D. Denney, "Wellbore-stability assessment for self-killing blowouts," *Journal of Petroleum Technology*, vol. 65, pp. 105–110, 1 2013.

[25] J. Ji, S. Jin, and C. G. Tinney, "Forming close-in earth-like planets via a collision-merger mechanism in late-stage planet formation," *The Astrophysical Journal*, vol. 727, pp. L5–, 12 2010.

[26] E. M. Rossi, G. Lodato, P. J. Armitage, J. E. Pringle, and A. J. King, "Black hole mergers: the first light," *Monthly Notices of the Royal Astronomical Society*, vol. 401, pp. 2021–2035, 1 2010.

[27] T. Al-Adwani, S. K. Singh, B. Khan, J. Dashti, G. Ferroni, A. Martocchia, and J. Estarabadi, "Real time advanced surface flow analysis for detection of open fractures," *SPE Europec/EAGE Annual Conference*, 6 2012.

[28] T. Elshehabi and I. Bilgesu, "Impact of drilling with oil based mud on well control in horizontal shale gas wells," in *SPE Eastern Regional Meeting*, SPE, 10 2015.

[29] K. Bybee, "Drilling underbalanced from a drillship in the santos basin," *Journal of Petroleum Technology*, vol. 58, pp. 74–76, 4 2006.

[30] X. Li, B. Zhang, J. Chen, T. Qi, B. Wang, and S. Chen, "The therapy of high-flow priapism by superselective internal pudendal artery embolisation," *Heart*, vol. 97, pp. A243.1–A243, 10 2011.

[31] H. F. Spoerker, C. Gruber, and W. Brandstaetter, "Dynamic modelling of gas distribution in the wellbore during kick situations," *IADC/SPE Drilling Conference and Exhibition*, 3 2012.

[32] G. Szekely, E. Peixoto, Z. Czovek, and T. Mezo, "Managed pressure drilling flexible mud return line advances," in *IADC/SPE Managed Pressure Drilling & Underbalanced Operations Conference & Exhibition*, SPE, 3 2017.

[33] M. S. M. Yusof, K. A. Khazali-Rosli, N. N. Ezzatty, P. Prasertamporn, M. Arathoon, S. Sockalingam, C. C. Hwa, and E. A. Muhamad, "Successful implementation of narrow margin drilling procedures to optimise a deepwater well," in *Offshore Technology Conference Asia*, OTC, 3 2018.

[34] C. Carpenter, "Managed-pressure-drilling equipment augments deepwater well control," *Journal of Petroleum Technology*, vol. 71, pp. 72–74, 1 2019.

[35] S. Sangesland, A. Sivertsen, and E. Hiorth, "Downhole blowout preventer," in *SPE/IADC Drilling Conference*, SPE, 3 1991.

[36] J. Li, J. Zhang, P. Luo, Y. Xiao, and L. He, "Case history: High density weighted polymer drilling fluid used in the deepest horizontal well dan 21 in sichuan basin of china," in *International Conference on Horizontal Well Technology*, SPE, 11 1996.

[37] H. Zhou, H. Fan, H. Wang, X. Niu, and G. Wang, "A novel multiphase hydrodynamic model for kick control in real time while managed pressure drilling," in *SPE/IADC Middle East Drilling Technology Conference and Exhibition*, SPE, 1 2018.

[38] H. C. Karlsen and T. Nilsen, "Live pressure control risk analysis for drilling through multiple reservoirs," in *International Petroleum Technology Conference*, IPTC, 1 2014.

[39] H. H. Al-Sharji, E. Ferdiansyah, S. Kumar, and F. A. Neyaei, "Challenges for coiled tubing in slim hole horizontal well intervention," in *Asia Pacific Oil and Gas Conference & Exhibition*, SPE, 8 2009.

[40] K. K. Fjelde, J. Frøyen, and A. A. Ghauri, "A numerical study of gas kick migration velocities and uncertainty," in *SPE Bergen One Day Seminar*, SPE, 4 2016.

[41] G. Bone, S. S. Janwadkar, W. John, and M. Isbell, "Mature field benefits from application of high-end technology," *SPE/IADC Drilling Conference*, 2 2005.

[42] E. Vefring, R. Rommetveit, and E. Borge, "An advanced kick simulator operating in a user-friendly x-window system environment," in *Petroleum Computer Conference*, SPE, 6 1991.

[43] M. Jellison and E. Klementich, "An expert system for casing string design," in *Petroleum Computer Conference*, SPE, 6 1990.

[44] A. Johnson, B. Piccolo, H. Pinkstone, B. Anderson, and J. Fraczek, "Augmenting deepwater well control with managed pressure drilling equipment," in *SPE/IATMI Asia Pacific Oil & Gas Conference and Exhibition*, SPE, 10 2017.

[45] J. Brakel, B. Tarr, W. Cox, F. Jorgensen, and H. V. Straume, "Smart kick detection; first step on the well control automation journey," *SPE/IADC Drilling Conference and Exhibition*, 3 2015.

[46] R. Rommetveit, K. Bjorkevoll, G. Bach, B. Aas, J. Hy-Billiot, R. Maglione, and P. Gie, "Full scale kick experiments in horizontal wells," *SPE Annual Technical Conference and Exhibition*, 10 1995.

[47] F. Shanks, D. Hammett, and H. Zinkgraf, "Experience drilling in deepwater high current areas," in *Offshore Technology Conference*, OTC, 4 1979.

[48] H. Patil, T. L. Ponder, M. A. Arnone, and D. M. Hannegan, "Advancing the mpd influx management envelope ime: A comprehensive approach to assess the factors that affect the shape of the ime," in *SPE/IADC Managed Pressure Drilling and Underbalanced Operations Conference and Exhibition*, SPE, 4 2018.

[49] B. J. Gedge, C. Y. Tan, J. Rao, H. K. D. Singh, J. Oracion, B. T. Quoc, V. B. Nguyen, N. H. Tran, T. L. T. Minh, R. J. Buitenhuis, L. D. Tran, A. E. Wittry, P. Malpas, A. Beaugeois, N. N. Huu, and N. V. Que, "The deployment of managed pressure drilling technology, to assist in the development of offshore hpht gas condensate fields in vietnam - planning, engineering, and implementation.," in *SPE Asia Pacific Oil & Gas Conference and Exhibition*, SPE, 10 2014.

[50] R. J. Lunn, "Options for scotland's gas future," 6 2015.

[51] S. Z. Luan, X. Sun, K. L. Wang, and A. X. Geng, "Summary in research on kick detection technology," *Advanced Materials Research*, vol. 821-822, pp. 1422–1425, 9 2013.

[52] D. V. Slyke and E. Huang, "Predicting gas kick behavior in oil-based drilling fluids using a pc-based dynamic wellbore model," *IADC/SPE Drilling Conference*, 2 1990.

[53] H. Gomm and L. Peters, "Steerable bhas drill storage wells with difficult trajectories. [bottom hole assembly]," *Oil & Gas Journal*, 7 1993.

[54] T. Elshehabi and I. Bilgesu, "Well integrity and pressure control in unconventional reservoirs: A comparative study of marcellus and utica shales," in *SPE Eastern Regional Meeting*, SPE, 9 2016.

[55] K. Manikonda, A. R. Hasan, A. Barooah, N. H. Rahmani, M. El-Naas, A. K. Sleiti, and M. A. Rahman, "A mechanistic gas kick model to simulate gas in a riser with water and synthetic-based drilling fluid," in *Abu Dhabi International Petroleum Exhibition and Conference*, p. D012S116R009, SPE, 2020.

[56] M. J. Graham, K. E. S. Ford, B. McKernan, N. P. Ross, D. Stern, K. B. Burdge, M. W. Coughlin, S. G. Djorgovski, A. J. Drake, D. A. Duev, M. M. Kasliwal, A. Mahabal, S. van Velzen, J. Belecki, E. C. Bellm, R. Burruss, S. B. Cenko, V. Cunningham, G. Helou, S. R. Kulkarni, F. J. Masci, T. A. Prince, D. J. Reiley, H. Rodriguez, B. Rusholme, R. Smith, and M. T. Soumagnac, "Candidate electromagnetic counterpart to the binary black hole merger gravitational wave event s190521g," *Physical review letters*, vol. 124, pp. 251102–, 6 2020.

[57] B. T. H. Marbun and A. M. I. Shidiq, "Estimation of annulus pressure fluids kick for vertical well using moore method and integrated numerical simulation," in *North Africa Technical Conference and Exhibition*, SPE, 4 2013.

[58] R. Green and C. Korzekwa, "Dewatering a deep gas well with a gas lift system-a case history," in *Permian Basin Oil and Gas Recovery Conference*, SPE, 3 1984.